Journal of University of Science and Technology Beijing
Vol.8(2001), No.1, p.48

Materials

Design and Synthesis of Ti-ZrO_2 Functionally Graded Materials

Lidong Teng, Fuming Wang, Wenchao Li

Metallurgy School, University of Science and Technology Beijing, Beijing 100083, China
(Received 2000-03-07)

Abstract: Functionally graded materials (FGMs) based on titanium-zirconia system have been prepared by powder metallurgical method. The graded interlayer number and the compositional distribution have been designed by elastic finite element method. The interfacial microstructure between layers, the combining state of phases between Ti and ZrO_2 have been investigated by means of XRD (X-ray diffraction), SEM (scanning electron microscope), EDS (energy dispersive spectrometer) and so on. The co-existing region of Ti and ZrO_2 has been determined by thermodynamic calculation to control the sintering atmosphere. The experimental results show that the joint between Ti and ZrO_2 phases is physical in this composite and ZrO_2 mainly exists as tetragonal phase. The microstructure of Ti-ZrO_2 system FGM exhibits a transition from a zirconia particle dispersion in a titanium matrix to an inverse dispersion of titanium in zirconia. The gradient structure of titanium and zirconia can relieve thermal stress.

Key words: Ti-ZrO_2 system; functionally graded material; thermodynamic analysis; finite element method

Functionally gradient materials (FGMs) have received considerable attention in recent years [1–3]. In FGMs, the gradient changes of composition and microstructure can reduce or eliminate specific interfaces between constituent materials, such as ceramics and metals. These features of FGMs are expected to relieve the residual stress, as well as to control thermal barrier characteristics. In this paper, $3Y_2O_3$-doped ZrO_2 (TZP) (mole fraction in %) was chosen as the candidate ceramic material, which has excellent thermal barrier property, anti-corrosion and wear resistance. Titanium metal is an important aerospace material which has high-temperature strength, thermal shock resistance and anti-corrosion, etc. This Ti-ZrO_2 system FGM was chosen on the basis of the potential applications in aerospace industries. As we know, various techniques have been employed in the preparation of FGMs [4], including physical and chemical vapor deposition, plasma spraying, sequential slipcasting, laser cladding, self-propagating high-temperature synthesis. Powder metallurgical (P/M) process is one of the most viable methods for the preparation of FGMs [5], which needs no extraordinary special equipment. The composition and the microstructure as well as the shape forming of FGM can be easily controlled in a wide range. Therefore, Ti-ZrO_2 system FGMs have been prepared by powder metallurgical (P/M) method. A wide temperature deviation between the inner and the outer surfaces is built up in materials that are applied to aerospace industries.

1 Optimization of Graded Microstructure

The disk-shaped specimen designed in this paper had a diameter of 50 mm and thickness of 9 mm, as shown in **figure 1**. To optimize the graded distribution of composition, finite element numerical models are utilized to study residual stress developed at graded ceramic-metal interfaces during cooling from the fabrication temperature. **Figure 2** shows the effect of the graded layer number on the relative maximum stresses (relative to the peak stress calculated for the non-graded interface). Note that for a given graded function expo-

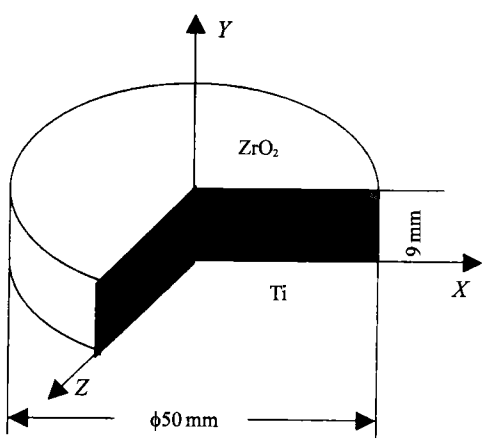

Figure 1 Geometrical model of the designed Ti-ZrO_2 FGM specimen.

nent, $p=1$, the stress decreases with increasing the interlayer number. It is demonstrated that the residual stresses were significantly reduced in the graded materials. However, when the graded number is more than 7, the stress decreases slightly with the increase of interlayer number. This result suggests that an optimum graded microstructure is one in which the interlayer number is more than 7. To simplify the preparing process, nine-layer graded specimen with equal-thickness layer has been designed in this experiment.

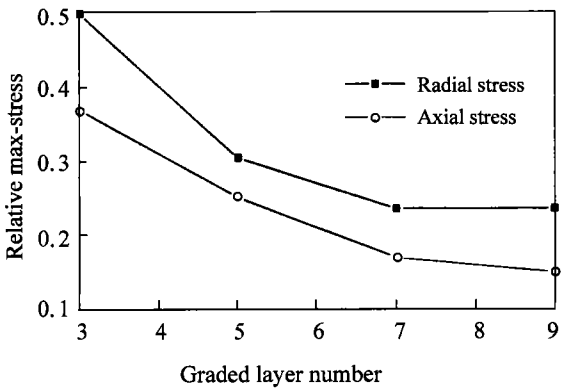

Figure 2 Effect of the graded layer number on the relative maximum stresses.

2 Experimental Procedure

The starting materials were $3Y_2O_3$-doped (mole fraction in %) tetragonal zirconia polycrystal (TZP) and titanium powders. TZP and Ti were mixed in alcohol with 12.5% (volume fraction) compositional gradient, and then ball-milled for 6.0 h with TZP milling media. The green bodies of each composition were fabricated at an optimized pressure using a disc-type steel die. When the content of the metal was above 75% (volume fraction), 1.0 (mass fraction) polyvinyl alcohol (PVA) was added for forming green bodies. The prepared disc-type green bodies of each composition were stacked in a graphite sleeve and hot pressed at 1400–1500 ℃ under a pressure of 25 MPa for 1.5–2.0 h in argon atmosphere and at 5.0 ℃/min on heating and cooling to relax the residual stress. The subsequent rate of cooling and unloading must be suitably controlled to prevent the sintered body from warping and cracking. Samples for microstructure inspection were cut with a diamond saw, and their surfaces were ground and polished. The hardness and Young modulus of FGM were measured by nanoindenter (Nano Indenter II). The density was measured by the Archimede's method. The compositional continuity via the distribution of metal elements was examined with an electron probe microanalyser (Link AN10000), and the microstructure and fractured surface morphology were observed by scanning electron microscopy (SEM, S-250MK3).

3 Results and Discussion

3.1 Thermodynamic analysis of Ti-Zr-O-N-C system

Titanium is an active metal, which can react easily with N_2, O_2, C, and H_2. Therefore, it is very important to select suitable sintering conditions for the synthesis of Ti-ZrO_2 system composites. Thermodynamic data of Ti-O-N, Zr-O-N, Ti-O-C and Zr-O-C have been calculated according to the JANAF Thermo-chemical Tables [6]. **Figure 3** shows the superimposed equilibrium phase diagram of Ti-O-N and Zr-O-N system at 1800 K, and **figure 4** shows that of Ti-O-C and Zr-O-C system at 1800 K. The relations between equilibrium of

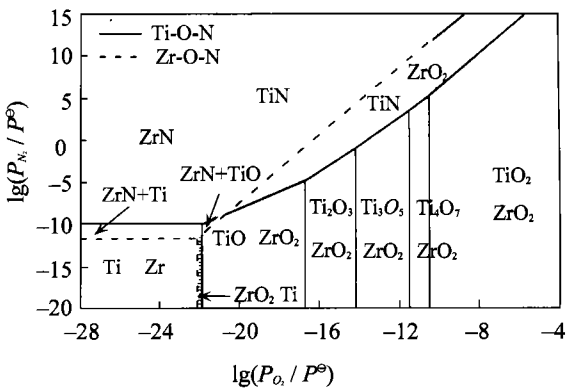

Figure 3 The superimposed equilibrium phase diagram by the Ti-O-N and Zr-O-N system at 1800 K.

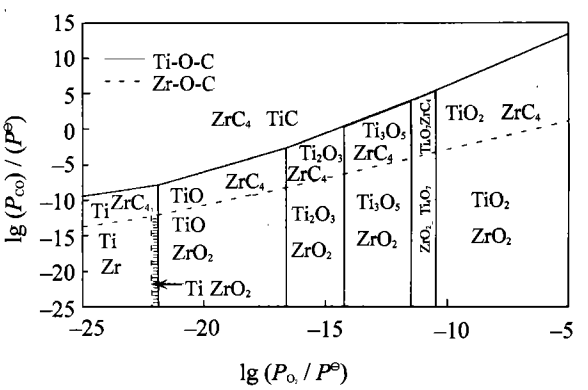

Figure 4 The superimposed equilibrium phase diagram by the Ti-O-C and Zr-O-C system at 1800K.

phases and partial pressure in Ti-Zr-O-N and Ti-Zr-O-C systems at 1800 K are shown in **table 1**. Obviously, to prevent oxidation or nitridation of titanium metal, partial pressure of oxygen P_{O_2} and nitrogen P_{N_2} must be less than 1.59×10^{-23} MPa and 1.63×10^{-11} MPa, respectively. The co-existing region of Ti and ZrO_2 is so narrow, $7.26\times10^{-24} < P_{O_2} < 1.59\times10^{-23}$ MPa, $\lg(p_{CO}/p^{\ominus}) < 3/4 \lg(p_{O_2}/p^{\ominus}) + 4.299$, $\lg(p_{N_2}/p^{\ominus}) < \lg(p_{O_2}/p^{\ominus}) +$

Table 1 The relations between phase equilibrium and partial pressure in Ti-Zr-O-N and Ti-Zr-O-C systems at 1800K

Chemical reactions	Equilibrium partial pressure
$Ti(s)+0.5O_2(g)=TiO(s)$	$\lg(p_{O_2}/p^{\ominus})=-21.798$
$Ti(s)+0.5N_2(g)=TiN(s)$	$\lg(p_{N_2}/p^{\ominus})=-28.000$
$Ti(s)+CO(g)=0.5O_2(g)+TiC(s)$	$\lg(p_{CO}/p^{\ominus})=0.5\lg(p_{O_2}/p^{\ominus})+3.100$
$Zr(s)+O_2(g)=ZrO_2(s)$	$\lg(p_{O_2}/p^{\ominus})=-22.139$
$Zr(s)+0.5N_2(g)=ZrN(s)$	$\lg(p_{N_2}/p^{\ominus})=-11.583$
$Zr(s)+4CO(g)=2O_2(g)+ZrC_4(s)$	$\lg(p_{CO}/p^{\ominus})=0.5\lg(p_{O_2}/p^{\ominus})-1.232$
$ZrN(s)+O_2(g)=0.5N_2(g)+ZrO_2(s)$	$\lg(p_{N_2}/p^{\ominus})=\lg(p_{O_2}/p^{\ominus})+32.6712$
$ZrC_4(s)+3O_2(g)=4CO(g)+ZrO_2(s)$	$\lg(p_{CO}/p^{\ominus})=(3/4)\lg(p_{O_2}/p^{\ominus})+4.299$

32.671 2, that super-purity argon must be used to control the sintering atmosphere, and the samples must be embedded in a particular powders.

In the co-existing region of Ti and ZrO_2 phases, the possible chemical reactions and their standard reaction Gibbs free energies are listed as follows:

$$Ti(s)+ZrO_2(s)=TiO_2(s)+Zr(s) \quad (1)$$

$$\triangle_r G_1^{\ominus}=160.154-0.010\,32\,T\,(kJ)$$

When $\triangle_r G_1^{\ominus}=0$, $T=15518.8$ K.

$$2Ti(s)+ZrO_2(s)=2TiO(s)+Zr(s) \quad (2)$$

$$\triangle_r G_2^{\ominus}=23.131-0.00801\,T\,(kJ)$$

When $\triangle_r G_2^{\ominus}=0$, $T=2887.765$ K.

The calculations show that Ti can not react with ZrO_2 in the range of sintering temperatures. Providing that Ti itself can not react with other gases, Ti/ZrO_2 graded composites can be obtained according to the thermodynamic analysis.

3.2 Properties of Ti-ZrO_2 composites

Figure 5 shows the density and the relative density of each gradient layer pressureless-sintered at the same temperature. The result reveals that the densification of samples was incomplete, although the densification of pure ZrO_2 and pure Ti were greater than the Ti-ZrO_2 composites. The difference between theoretical and practical densities is caused by the pores existing in the sintered body. It can be expected that these pores will cause the relaxation of residual stress and improve the thermal properties from the viewpoint of thermal protection and thermal shock resistance [7]. However, the control of porosity is required because of the degradation of mechanical properties.

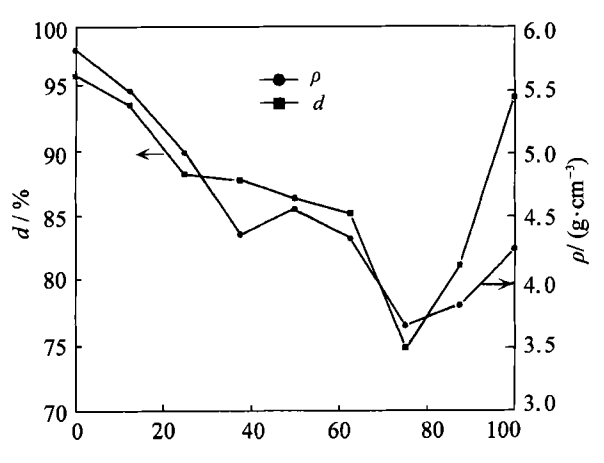

Figure 5 Density (ρ) and relative density (d) of Ti-ZrO_2 composite pressureless-sintered at 1873K.

Figure 6 shows the Vicker hardness of Ti-ZrO_2 composites with various Ti volume fractions pressureless-sintered at 1873 K. The hardness values are inversely proportional to metal volume fraction, because the metal has relatively low hardness values. However, the hardness is influenced by the sintering density and the intrinsic material properties [8]. When the volume fraction of Ti is more than 75%, the hardness increases with the increase of Ti content due to the increase of the sintering density (as shown in figure 5). **Figure 7** shows the Vicker hardness and Young modulus of each graded layer in Ti-ZrO_2 FGM hot-pressed at 1673 K. The values of hardness and Young modulus are all decreased with the increase of Ti content, because Ti metal has relatively lower hardness and modulus compared with those of ZrO_2. The hardness value of hot-pressed sam-

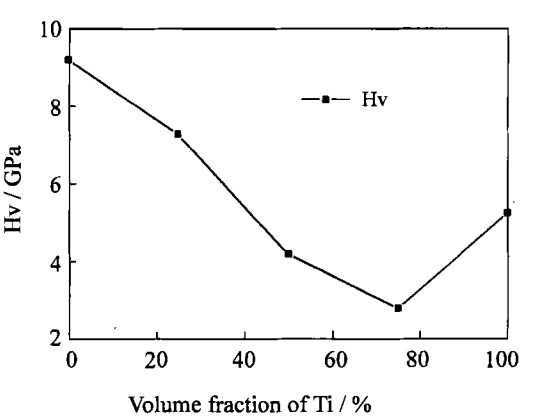

Figure 6 Effect of Ti volume fraction on Vicker hardness in Ti-ZrO_2 composite pressureless-sintered at 1873K.

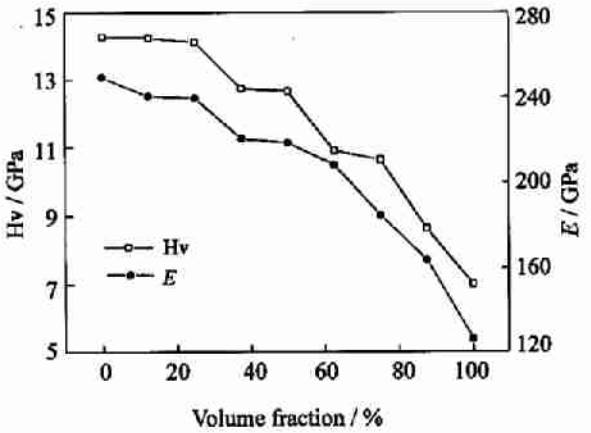

Figure 7 The Vicker hardness and Young modulus of each graded layer in Ti-ZrO_2 FGM hot-pressed at 1673K.

ples is higher than that of pressureless-sintered samples, since the hot-pressed sample has higher density than the pressureless-sintered sample with the same composition.

3.3 Phase composition and microstructure

The X-ray diffraction patterns of different layers in Ti-ZrO_2 system FGMs indicate that the phase composition consists of titanium, tetragonal zirconia (t-ZrO_2) and a little monoclinic zirconia (m-ZrO_2) as shown in **figure 8.** It is evident that there is no reaction between Ti and ZrO_2 in hot-pressing process. This result is in accordance with the thermodynamic calculations in section 3.1.

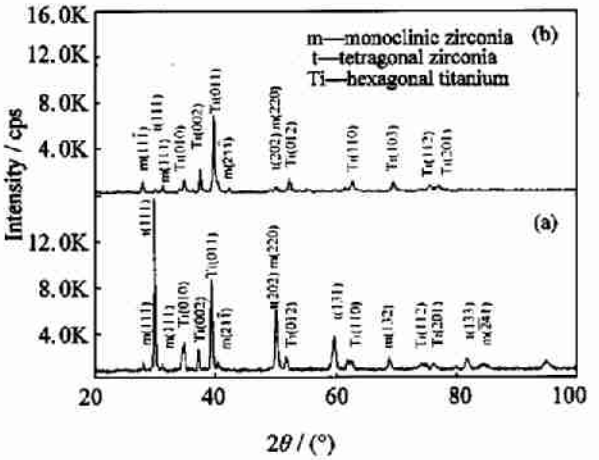

Figure 8 X-ray diffraction patterns of different layers in Ti - ZrO_2 system, (a) 50% Ti; (b) 75% Ti (volume fraction).

The scanning electron micrographs, using back-scattered electron image (BEI), of a polished section of the FGM samples and the EDS analysis of phase composition (titanium) are represented in **figure 9** and **figure 10,** respectively. It has been shown that despite stepwise stacking, the microstructure and the distribution of phase composition are gradually changed without distinct boundaries between the layers. The white phase is zirconia and the dark titanium. This can be verified by the EDS analysis in figure 9(d) and figure

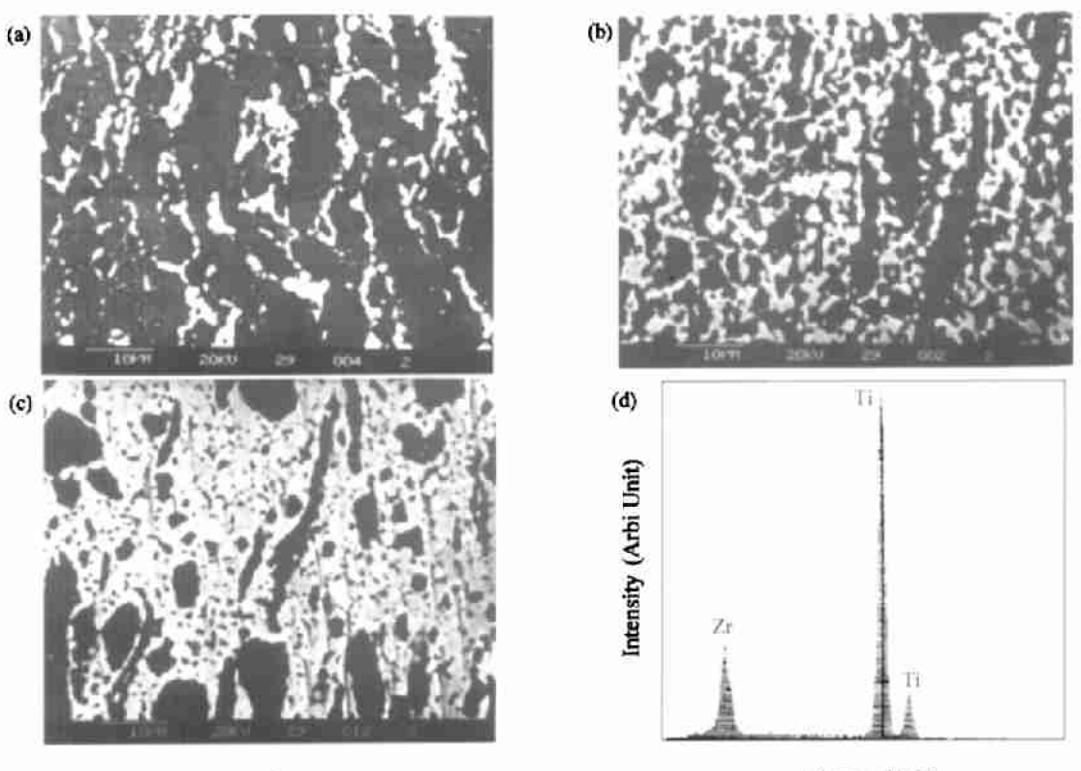

Figure 9 Backscattered electron image of cross-sectional multilayer structure in Ti-ZrO_2 FGM with 12.5% variation, (a) 75% Ti; (b) 50% Ti; (c) 25%Ti (volume fraction); (d) The EDS of black phase in figure 9(c).

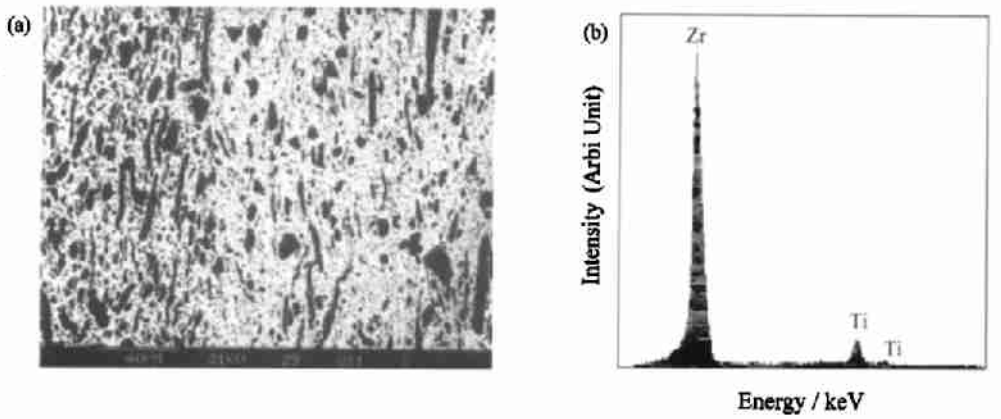

Figure 10 Microstructure of gradient layers and EDS of phase composition, (a) Interfacial microstructure between 37.5% Ti and 25% Ti layer (volume fraction); (b) The EDS of white phase in figure 10(a).

10(b). It is observed that the microstructure gradually changes from titanium to zirconia with variation in composition, and distinct boundaries, such as those in Ti-ZrO_2 direct bonding, disappear. It should be noted that the structures of Ti-ZrO_2 system FGM are microscopically inhomogeneous because of the coexistence of several different phases. However, the composition and the microstructure of Ti-ZrO_2 system FGM gradually change from one area to another so that they are continuous both in composition and structure, as shown in figure 10(a). Meanwhile, the SEM photographs exhibit a microstructure transition as shown in figure 9. In the titanium rich region, the FGM has a dispersed microstructure with ZrO_2 particles in the titanium matrix (figure 9 (a)). Typical network structures of titanium can be seen in the microstructures for 50Ti (volume fraction in %) (figure 9(b)). As the ZrO_2 content increases to 75 (volume fraction in %), the microstructure changes to an inverse dispersion in which the titanium particles are almost discretely distributed in the ZrO_2 matrix (figure 9 (c)). Thus there is no macroscopic interface in the FGM. This is the difference between Ti-ZrO_2 system FGM and direct bonding of the two materials. As a result, Ti-ZrO_2 system FGM will have the dual advantages of ceramics and metals for practical purposes, and they will be free from fracture of spallation which occurs for metal/ceramic interfaces, giving a reduction in thermal stress.

4 Conclusions

(1) The graded microstructure is optimized by finite element numerical modeling analysis. Nine-layer FGMs based on titanium-zirconia system have been prepared by powder metallurgical method.

(2) The sintering atmosphere must meet the following conditions determined by thermodynamic calculations to prepare Ti-ZrO_2 system composites: $7.26\times10^{-24} < p_{O_2} < 1.59\times10^{-23}$ MPa, $p_{N_2} < 1.63\times10^{-11}$ MPa, $\lg(p_{CO}/p^{\ominus} < 3/4\lg(p_{O_2}/p^{\ominus}) + 4.299$.

(3) Titanium and zirconia components are continuous in microstructure. There is no distinct interface in the FGM due to the gradient changes of composition and structure. Moreover, with the compositional variation, the microstructure of Ti-ZrO_2 system FGM exhibits a transition from a zirconia particle dispersion in a titanium matrix to an inverse dispersion of titanium in zirconia.

(4) The sintered Ti-ZrO_2 system FGM body consists of titanium, tetragonal zirconia (t-ZrO_2) and a little monoclinic zirconia (m-ZrO_2). No reaction product between Ti and ZrO_2 is detected, and the Ti/ZrO_2 phase interfaces may be directly connected.

Acknowledgement

This work was supported by the National Natural Science Foundation of China (No.59872002).

References

[1] A. Mortensen, S. Suresh: *International Material Reviews*, 40 (1995), p. 239.
[2] A. J. Markworth, K. S. Ramesh, W. P. Parks: *J. Mater. Sci.*, 30 (1995), p. 2183.
[3] L. M. Zhang, X. F. Tang, Y. Z. Yuan: *J. Chinese Ceram. Soc.*, 21 (1993), No. 5, p. 406.
[4] A. J. Ruys, J. A. Kerdic, C. C. Sorrell: *Journal of Materials Science*, 31 (1996), p. 4347.
[5] A. Kawasaki, R. Watanabe: *J. Jpn. Soc. Powder and Powder Metall.*, 37 (1990), p .253.
[6] JANAF: *Thermodynamical Tables*, 3rd edition, R. David, Jr. Lide [ed.], Thermal Group, 1707 Building, Dow Chemical U.S.A., Midland, MI48674, USA, 1985, P. 42.
[7] R. Watanabe, A. Kawask: *J. Jpn Soc. Powder and Powder Metall.*, 39 (1992), p. 279.
[8] Y. G. Jung, S. C. Chol, U. G. Paik: *J. Mater. Sci.*, 32 (1997), p. 3841.